

Distribution and Dynamics of ^{99m}Tc -Pertechnetate Uptake in the Thyroid and Other Organs Assessed by Single-Photon Emission Computed Tomography in Living Mice

Philippe R. Franken,¹ Julien Guglielmi,¹ Christian Vanhove,² Malick Koulibaly,¹ Michel Defrise,² Jacques Darcourt,¹ and Thierry Pourcher¹

Background: ^{99m}Tc pertechnetate is a well-known anion, used for clinical imaging of thyroid function. This gamma emitter is transported by the sodium iodide symporter but is not incorporated into thyroglobulin. Scintigraphy using ^{99m}Tc pertechnetate or ^{123}I iodide represents a powerful tool for the study of sodium iodide symporter activity in different organs of living animal models. However, in many studies that have been performed in mice, the thyroid could not be distinguished from the salivary glands. In this work, we have evaluated the use of a clinically dedicated single-photon emission computed tomography (SPECT) camera for thyroid imaging and assessed what improvements are necessary for the development of this technique.

Methods: SPECT of the mouse neck region, with pinhole collimation and geometric calibration, was used for the individual measurement of ^{99m}Tc pertechnetate uptake in the thyroid and the salivary glands. Uptake in the stomach was studied by planar whole-body imaging. Uptake kinetics and biodistribution studies were performed by sequential imaging.

Results: This work has shown that thyroid imaging in living mice can be performed with a SPECT camera originally built for clinical use. Our experiments indicate that ^{99m}Tc pertechnetate uptake is faster in the thyroid than in the salivary glands and the stomach. The decrease in ^{99m}Tc pertechnetate uptake after injection of iodide or perchlorate as competitive inhibitors was also studied. The resulting rate decreases were faster in the thyroid than in the salivary glands or the stomach.

Conclusions: We have shown that a clinically dedicated SPECT camera can be used for thyroid imaging. In our experiments, SPECT imaging allowed the analysis of ^{99m}Tc pertechnetate accumulation in individual organs and revealed differences in uptake kinetics.

Introduction

THYROID HORMONE PRODUCTION is a multistep process. The sodium iodide symporter (NIS), located in the basolateral membrane of the thyrocyte, accumulates iodide from the blood stream into the cells (1). Iodide then diffuses through the apical membrane and is incorporated into organic molecules, the thyroglobulins. These iodinated organic molecules are phagocytosed and hydrolyzed into triiodothyronine and thyroxine hormones, which are released into the blood stream.

NIS is not only found in the thyroid but is also expressed in the stomach and the salivary glands (2), where it mediates iodide accumulation. This process may be part of the host defense to microbe-containing food contaminants.

During the period 1940–1960, radioactive iodide was used in animal experiments (mostly rats) and proved to be useful for the understanding of thyroid function and regulation. Subsequently, thyrocyte regulation was studied in *in vitro* experiments on primary cultures and cell lines derived from thyroid cells. However, animal experiments are still required for a better knowledge of thyroid function and regulation. This is of particular interest since the development of genetically modified mice, which represent powerful tools for such investigations.

For several decades, thyroid scintigraphy has been a well-established technique for the diagnosis of thyroid pathologies, but it has not been often used in animal experiments. Radioactive ^{123}I iodide or ^{131}I iodide is used in recording the uptake of free iodide and incorporated iodine. Several gamma emitters

¹Transporters, Imaging and Radiotherapy in Oncology (TIRO), Commissariat Energie Atomique Direction des Sciences du Vivant (DSV)-institut de Biologie Environnementale et Biotechnologie (iBEB)-Service de Biochimie et Toxicologie Nucléaire (SBTN), Centre Antoine Lacassagne, University of Nice Sophia Antipolis, Nice, France.

²In vivo Cellular and Molecular Imaging Center (ICMIC), Vrije Universiteit Brussel, Brussels, Belgium.

are substrates of NIS and are actively accumulated in the thyroid. One of these, ^{99m}Tc pertechnetate ($^{99m}\text{TcO}_4$), is transported by NIS but it is not incorporated into thyroglobulin (TG) and, therefore, allows the specific study of uptake capacity.

For mouse imaging, resolution is an important issue, to distinguish the different organs that are capable of iodide accumulation. Some of these organs are very small. For example, the size of a mouse thyroid lobe is approximately $1\text{ mm} \times 0.3\text{ mm}$. In addition, organs that accumulate radioactive ^{99m}Tc pertechnetate can be very close to each other, that is, the salivary glands and the thyroid. Consequently, radioactive ^{99m}Tc pertechnetate uptake into these two organs may be superimposed in the same image. It is therefore mandatory to use tomography (single-photon emission computed tomography [SPECT]) with improved spatial resolution.

Large rotating clinical cameras are a low-cost alternative to dedicated microSPECT systems for small animal imaging. However, these large rotating cameras are subject to mechanical irregularities, which may have deleterious effects on spatial resolution because of the magnifying effect of pinhole collimation. Earlier work using pinhole SPECT for small animal imaging was based on simple calibration methods that only estimated a few parameters, such as the center of rotation, the focal length, and the radius of rotation (3). More accurate calibration techniques have been developed and submillimetric spatial resolution has been reported by several groups using different types of single and multiple pinhole collimators (4,5) and slit-slat collimators (6).

A new calibration method has been proposed recently (7). This method refines an initial parametric calibration (8,9) by applying to each position of the camera a rigid body transformation that is determined to improve the fit between the measured and the calculated projections of the calibration sources. A stable estimate of this transformation can be obtained with only three calibration sources by linearizing the equations around the position estimated by the initial parametric calibration.

In this study, this new method was used for imaging the thyroid in mice using ^{99m}Tc pertechnetate. We analyzed the spatial distribution of ^{99m}Tc pertechnetate uptake and its dynamics in the thyroid, the salivary glands, and the stomach. We also studied ^{99m}Tc pertechnetate discharge following excess administration of perchlorate and iodide.

Methods

Animals and study protocol

Male, wild-type mice (C57 BL6/6J) were purchased from Charles River (L'arbresle, France). At the time of the experiments, the mice were between 6 and 8 weeks old (25–30 g). Animals were fed a standard diet. The study protocol was approved by the Committee for Animal Studies and the National Institutes of Health Principles of Animal Laboratory Care (NIH publication 86–23, revised 1995).

About 250–300 MBq of ^{99m}Tc pertechnetate ($^{99m}\text{TcO}_4$) was injected intraperitoneally. After 10 minutes, animals were anesthetized and kept asleep during the complete imaging protocol using isoflurane gas (1.5 vol% in air). Pinhole SPECT imaging of the neck (nSPECT) began 20 minutes after $^{99m}\text{TcO}_4$ injection (nSPECT 1, Fig. 1) and was followed by whole-body planar imaging (wbPLANAR). Animals were then injected intraperitoneally with sodium chloride (2 mg NaCl), sodium

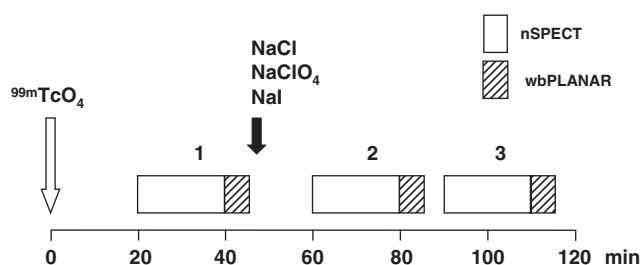


FIG. 1. Study protocol. After ^{99m}Tc pertechnetate injection, neck single-photon emission computed tomography imaging (nSPECT) followed by whole-body planar imaging (wbPLANAR) were performed three times. Animals were then injected intraperitoneally with sodium chloride (NaCl), sodium perchlorate (NaClO_4), or sodium iodide (NaI), immediately after the first total body planar imaging.

perchlorate (2 mg NaClO_4), or sodium iodide (2 mg NaI). Three animals were used for each experimental condition. Pinhole SPECT of the neck followed by wbPLANAR was repeated 10 minutes (nSPECT 2, wbPLANAR 2) and 40 minutes later (nSPECT 3, wbPLANAR 3).

Neck SPECT imaging

SPECT projection images of the mouse neck were obtained using a large field-of-view rotating gamma camera (Sopha DSX; Sopha Medical System, General Electric, Buc, France) equipped with a pinhole collimator with a 1 mm aperture. The acquisition parameters were 64 projections over 360° , circular orbit, and a 21 mm radius of rotation. The photopeak window was set at 126–154 keV. Data were collected in 128×128 pixel matrix with an acquisition zoom $2\times$, resulting in a 2.26 mm detector pixel size. The total acquisition time was 20 minutes (15 seconds for each projection).

The tomographic images were reconstructed by an iterative reconstruction algorithm based on the ordered subset expectation maximization scheme using three iterations in combination with eight subsets. The reconstruction algorithm incorporated (i) the pinhole geometry, (ii) the collimator response and (iii) the angular variation of the detector sensitivity (10).

The pinhole geometry was determined using the calibration method presented by Beque *et al.* (8,9) and recently refined by Defrise *et al.* (7). The technique first acquired circular orbit projection data of a three-point source phantom, which forms a triangle with known dimensions. The phantom was composed of three cylindrical holes, filled with $100\text{ }\mu\text{Ci}/\mu\text{L}$ ^{99m}Tc pertechnetate, of 1 mm diameter and 1 mm depth, drilled into a 4-mm-thick plexiglas plaque. The locations of the three sources on each projection image were then determined using simple segmentation techniques. The focal length of the pinhole collimator, the radius of rotation, the mechanical and electronic shifts, as well as the tilt and the twist of the detector were then determined for each projection by fitting iteratively the analytically calculated locations to the measured locations (8,9). The fit was further refined by applying a rigid body transformation to each position of the camera, as recently proposed by Defrise *et al.* (7). The collimator response was corrected using a multiray method (11), which models the finite dimension of the pinhole opening by calculating each data sample as the average of seven rays in the forward and backward projector of the reconstruction algorithm. The

angular variation of the sensitivity due to the pinhole collimator was corrected by acquiring a ^{99m}Tc pertechnetate flood source, which was positioned directly on the pinhole collimator surface. The measured sensitivity map was incorporated into the reconstruction process. There was no correction for partial volume, scatter, or attenuation.

The reconstructed data were stored in a 0.2-mm pixel-size matrix and postfiltered with a three-dimensional (3D) Gauss filter with a full-width at half maximum of 0.4 mm. Post-reconstruction spatial resolution measured on the Ultra-Micro Hot Spot Phantom (Data Spectrum Corporation, Chapel Hill, NC) using these acquisition and processing parameters was 1 mm.

wbPLANAR

Planar whole-body images of the mice in the anterior view were obtained with the pinhole opening located 10 cm from the body surface. Data were recorded during 300 seconds into a 128×128 matrix with 2.26 mm pixel size and corrected for the angular variation of the sensitivity of the detector using the measured sensitivity map described earlier.

Image analysis

SPECT image viewing and quantification were performed using AMIDE software (A Medical Image Data Examiner) (12). Images of the three SPECT studies obtained for each animal were analyzed side by side. 3D regions of interest (ROIs) were automatically drawn around the thyroid and the salivary glands of the first SPECT (nSPECT 1) by thresholding the image of each organ at 25% of the maximum pixel value in each organ. These ROIs were then used to measure ^{99m}Tc pertechnetate uptake in the thyroid and the salivary glands on the three nSPECT acquisitions, respectively. Uptake was calculated as counts in the tissue divided by the injected activity after decay correction. A pinhole SPECT acquisition of a 2-mL syringe containing 37 MBq/mL of ^{99m}Tc pertechnetate was performed as a reference for the conversion of injected activity into measured counts in the image.

The planar, whole-body image was used to quantify the uptake of ^{99m}Tc pertechnetate in the stomach. A ROI was drawn on the stomach using a threshold of 25% of the maximal activity. For each of the three acquisitions, counts in the stomach were normalized to the total body activity measured on the first acquisition (wbPLANAR 1) after decay correction.

Statistical analysis

Results are presented as mean \pm standard error of the mean. A two-tail paired *t*-test was used to determine the significance of changes in ^{99m}Tc pertechnetate uptake in organs.

Results

Spatial distribution of ^{99m}Tc pertechnetate uptake in living mice

According to our study protocol (Fig. 1), whole-body images of mice in the anterior view were first obtained 40–45 minutes (5 minutes acquisition) after intraperitoneal injection of ^{99m}Tc pertechnetate (Fig. 2A). Activities were predominantly located in the stomach, the bladder, and the neck region, but in these whole-body planar images the thyroid could not be clearly distinguished from the large salivary

glands. Resolution of the thyroid in planar imaging was significantly improved if the pinhole was positioned as close as possible to the thyroid. This can be illustrated by the first projection image (15 seconds/acquisition) of each SPECT acquisition, which corresponds to anterior views (Fig. 2B–D). The thyroid was then clearly observed with the acquisition that was performed almost immediately after ^{99m}Tc pertechnetate injection (20 minutes). The distinction between the thyroid and the salivary glands decreased progressively with time (nSPECT 1–3), because of increased accumulation in the salivary glands (compare Fig. 2B, C, and D). This effect was more important with whole-body images (wbPLANAR 1–3) (data not illustrated; only wbPLANAR 1 is shown in Fig. 2A).

In contrast, using tomographic images of the neck (nSPECT), easier distinction of the thyroid from the salivary glands was expected, especially using our refined calibration method. The two thyroid lobes were clearly visualized in coronal (Fig. 2E), sagittal (Fig. 2F), and transverse (Fig. 2G) slices from nSPECT 1 (20–40 minutes).

Dynamics of ^{99m}Tc pertechnetate uptake

From each nSPECT image, 3D ROIs were drawn around the thyroid and the salivary glands and $^{99m}\text{TcO}_4$ uptake was calculated for each organ. The ^{99m}Tc pertechnetate uptake in the thyroid averaged $1.87\% \pm 0.67\%$ of the initial dose (% ID) 20–40 minutes after ^{99m}Tc pertechnetate injection (nSPECT 1), $1.97\% \pm 0.74\%$ ID 60–80 minutes after ^{99m}Tc pertechnetate injection (nSPECT 2), and $1.86\% \pm 0.75\%$ ID 90–110 minutes after ^{99m}Tc pertechnetate injection (nSPECT 3) (Fig. 3A). This result indicates that $^{99m}\text{TcO}_4$ uptake in the thyroid quickly reaches a maximal value. As illustrated in Figure 3B, where the values are expressed as a percentage of the final ^{99m}Tc pertechnetate uptake, no increase was observed between nSPECT 1 and nSPECT 2 or 3 (Fig. 3B).

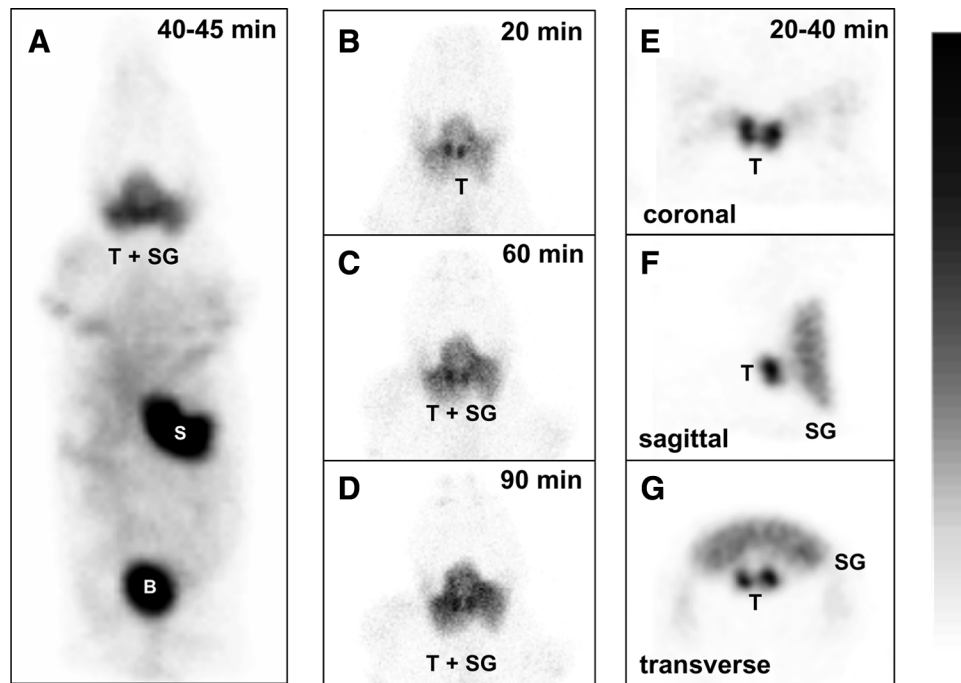
In contrast, ^{99m}Tc pertechnetate uptake in the salivary glands increased slightly, but significantly ($p < 0.05$), from $13.65\% \pm 5.1\%$ ID 20–40 minutes after ^{99m}Tc pertechnetate injection (nSPECT 1) to $18\% \pm 6.5\%$ ID 60–80 minutes after ^{99m}Tc pertechnetate injection (nSPECT 2) and further increased to $20.8\% \pm 7.3\%$ ID 90–110 minutes after ^{99m}Tc pertechnetate injection (nSPECT 3) (Fig. 3). These results indicate that the maximal value in ^{99m}Tc pertechnetate uptake is attained more gradually in the salivary glands (Fig. 3B).

The uptake of ^{99m}Tc pertechnetate in the stomach, measured on the whole-body planar images obtained immediately after SPECT imaging, averaged $30.6\% \pm 8.5\%$ ID 45–50 minutes after ^{99m}Tc pertechnetate injection (wbPLANAR 1). Activity increased to $34\% \pm 6.6\%$ ID 80–85 minutes after ^{99m}Tc pertechnetate injection (wbPLANAR 2) and to $37\% \pm 7\%$ ID 110–115 minutes after ^{99m}Tc pertechnetate injection (wbPLANAR 3) ($p < 0.05$, Fig. 3). This indicates that ^{99m}Tc pertechnetate uptake is slower in the stomach than in the thyroid.

Effect of sodium perchlorate and sodium iodide on ^{99m}Tc pertechnetate uptake in the thyroid, the salivary glands, and the stomach

We also analyzed the effects of competitive inhibitors on ^{99m}Tc pertechnetate uptake. Two inhibitors were used—perchlorate (ClO_4^-) and iodide (I^-)—which are both NIS substrates and are known to block ^{99m}Tc pertechnetate

FIG. 2. Left panel: Whole body imaging (A) of a normal mouse was obtained in anterior view with the pinhole at 10 cm from the body, 40–45 minutes after ^{99m}Tc pertechnetate injection. The image was calibrated to the maximal value in the thyroid. Middle panel: Neck anterior planar imaging (30 seconds acquisition) was obtained with the pinhole at 21 mm from the neck, 20 minutes (B), 60 minutes (C), and 90 minutes (D) after ^{99m}Tc pertechnetate injection (T, thyroid; SG, salivary glands; S, stomach; B, bladder). Images were calibrated to the maximal value of the dynamic series. Right panel: Coronal (E), sagittal (F), and transverse (G) slices of the thyroid (T) and the salivary glands (SG) obtained with pinhole SPECT in a control mouse, 20–40 minutes after ^{99m}Tc pertechnetate injection. Images were calibrated to the maximal value of the tomographic volume.



uptake. As illustrated in Figure 4, a rapid inhibition of ^{99m}Tc pertechnetate uptake in the thyroid and, to a lesser extent, in the salivary glands was observed in nSPECT 2 and 3. For the thyroid, ^{99m}Tc pertechnetate uptake decreased from the value obtained in nSPECT 1 (20–40 minutes) (set to 100%) to $35\% \pm 12\%$ (nSPECT 2, 60–80 minutes) and $22\% \pm 9\%$ (nSPECT 3, 90–110 minutes) after NaClO_4 injection or to $31\% \pm 7\%$ (nSPECT 2, 60–80 minutes) and $21\% \pm 5\%$ (nSPECT 3, 90–110 minutes) after NaI injection (Fig. 5, upper panel). For the salivary glands, ^{99m}Tc pertechnetate uptake decreased from the value obtained in nSPECT 1 (20–40 minutes) (set to 100%) to $64\% \pm 8\%$ (nSPECT 2, 60–80 minutes) and $45\% \pm 8\%$ (nSPECT 3, 90–110 minutes) after NaClO_4 injection or to $89\% \pm 4\%$ (nSPECT 2, 60–80 minutes) and $75\% \pm 4\%$ (nSPECT 3, 90–110 minutes) after NaI injection (Fig. 5, middle panel). The reason for the discrepancy between NaClO_4 and NaI is unknown. For the stomach, ^{99m}Tc pertechnetate uptake decreased from the value obtained in wbPLANAR 1 (40–45 minutes) (set to 100%) to $73\% \pm 10\%$ (wbPLANAR 2, 80–85 minutes) and $61\% \pm 13\%$ (wbPLANAR 3, 110–115 minutes) after NaClO_4 injection or to $77\% \pm 11\%$ (wbPLANAR 2, 80–85 minutes) and $70\% \pm 16\%$ (wbPLANAR 3, 110–115 minutes) after NaI injection (Fig. 5, lower panel).

Discussion

Our study indicates that NIS activity in different mouse organs can be studied *in vivo* using SPECT imaging and ^{99m}Tc pertechnetate. Tomography was required to distinguish between ^{99m}Tc pertechnetate uptake in the thyroid and its

uptake in the salivary glands. 3D visualization, at high resolution, of the thyroid was obtained with a SPECT camera originally dedicated to clinical applications. One millimeter spatial resolution was achieved with a custom-made pinhole collimator after geometric calibration of the camera. ^{99m}Tc pertechnetate uptake into the thyroid, the salivary glands, and the stomach of mice was analyzed. We found that ^{99m}Tc pertechnetate accumulation was slower in the salivary glands and the stomach compared with the thyroid. We also found that ^{99m}Tc pertechnetate efflux after iodide or perchlorate injection was slower in the salivary glands and the stomach compared with the thyroid. As the masses of the salivary gland and the stomach are larger than the mass of the thyroid, the percentages of the injected dose that accumulated are higher.

As has been well established in both humans and mice, three main tissue types accumulate ^{99m}Tc pertechnetate: the thyroid, the stomach, and the salivary glands. High NIS gene expression levels have been detected in these three organs (13,14), and this has been corroborated with immunohistochemical analyses (2,15). With respect to ^{99m}Tc pertechnetate uptake, it is important to point out that, besides NIS expression, tissue organization may play an important role. In the thyroid, the stomach, and the salivary glands, high NIS expression levels were found in epithelial cell-delimiting compartments: thyroid colloid, gastric lumen, and salivary acini and duct lumens, respectively. Consequently, ^{99m}Tc pertechnetate uptake in these organs is not only related to the radiotracer accumulation in NIS-expressing cells but also to the radiotracer accumulation into the corresponding compartments. We assume that the slower uptake and efflux rates in

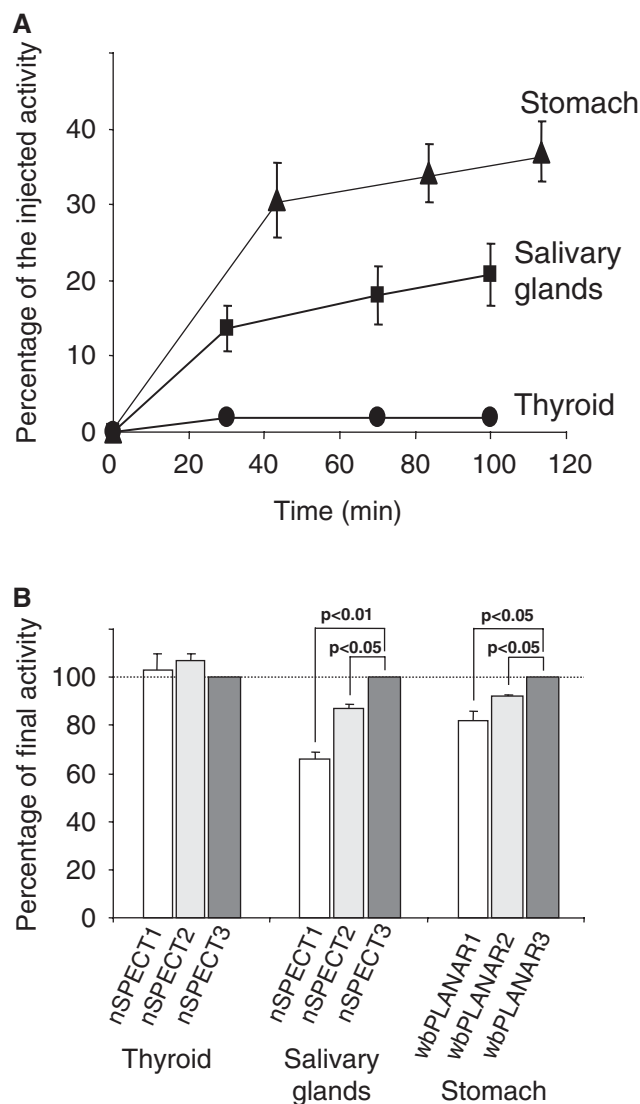


FIG. 3. Comparison of ^{99m}Tc pertechnetate uptake dynamics in the thyroid, the salivary glands, and the stomach. The values were calculated from nSPECT (for the thyroid and the salivary glands) or whole-body imaging (for the stomach). The values are shown as a percentage of the injected activity (A) or as a percentage of the final activity in each organ (B), calculated from nSPECT 3 or wbPLANAR 3. In (A), the time of each measurement corresponds to the middle of the acquisition. Each value was calculated from three independent experiments.

the salivary gland and the stomach are linked to compartments that are proportionally larger. These differences in the kinetics are independent of the mass of the tissue. If we compare the percentage of the injected dose in each organ, this is related to the mass of the organ, but also to several other parameters, such as (i) the capacity of the NIS-expressing cells to mediate an iodide accumulation that results from dissimilar NIS expression in the tissues; (ii) the diffusion of accumulated iodide into intraorgan compartments (e.g., much larger in the stomach than in the thyroid); (iii) the passive diffusion of the iodide through the epithelia delimiting the compartments; (iv)

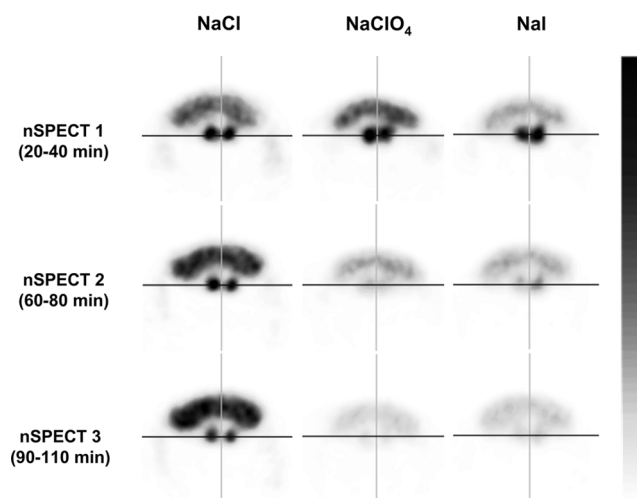


FIG. 4. Effect of NaClO_4 or NaI on the uptake of ^{99m}Tc pertechnetate in the thyroid and the salivary glands. Transverse slices of the thyroid and the salivary glands are shown before (nSPECT 1) and after (nSPECT 2 and nSPECT 3) injection of NaClO_4 or NaI . NaCl was used as the control (left slices). The images were calibrated to the maximal value in the thyroid at baseline, before injections (nSPECT 1).

the intake and output of the compartment (e.g., salivary secretion).

As shown in this work, our SPECT imaging procedure can distinguish between ^{99m}Tc pertechnetate uptake in the thyroid and the salivary glands. Many reports have described scintigraphic analyses of radioactive NIS substrates (^{123}I iodide, ^{125}I iodide, or ^{131}I iodide, ^{99m}Tc pertechnetate, ^{211}As astatine, or ^{188}Re perrhenate) in rodents. Most of these experiments were performed with a nontomographic gamma camera. Zuckier *et al.* reported an interesting and detailed *ex vivo* kinetic analysis of the tissue distribution of ^{123}I iodide, ^{99m}Tc pertechnetate, and ^{188}Re perrhenate by directly counting the accumulated radioactivity after organ removal (16). This analysis clearly showed the uptake activity of the salivary glands. These authors also studied the tissue distribution of the isotopes using *in vivo* imaging. It seems that the radiotracer detected in the neck region was attributed to thyroid uptake without considering the salivary glands. In other studies that did not focus on thyroid uptake, the authors have also considered radioactive accumulation in the mouse neck region to correspond to thyroid uptake [see examples with ^{99m}Tc pertechnetate (17) or ^{211}As astatine (18)].

In other studies, the salivary glands were not correctly localized on the *in vivo* gamma images. Isotope accumulation in the region of the animal's muzzle was related to the salivary glands (19,20). Using SPECT imaging, Cho *et al.* showed that signals obtained in this region could rather be attributed to isotope accumulation in the nasal mucosa (21).

This problem does not occur in rats because rat salivary glands do not accumulate iodide (22) and probably do not express NIS. Consequently, radioactive NIS substrate uptake in the rat neck region can be associated exclusively with thyroid uptake [see example in (23,24)].

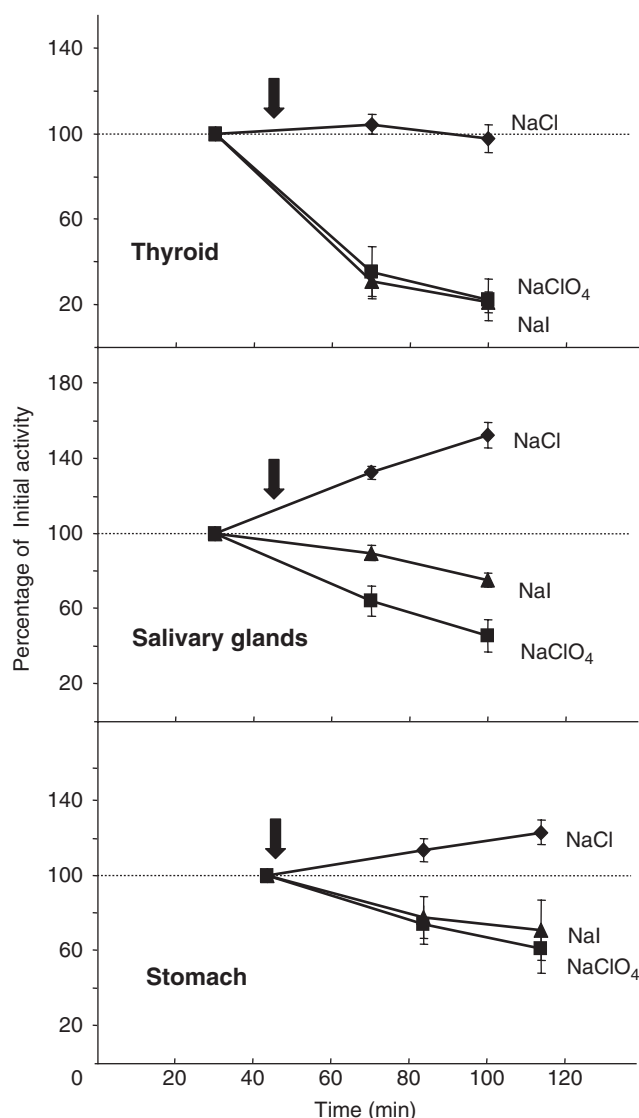


FIG. 5. Comparison of the effect of NaClO₄ or NaI on ^{99m}Tc pertechnetate uptake in the thyroid, the salivary glands, and the stomach. The values were calculated from SPECT (for the thyroid and the salivary glands) or whole-body imaging (for the stomach). The values are shown as a percentage of the initial activity accumulated in each organ, calculated from nSPECT 1 or wbPLANAR 1. The time of each measurement corresponds to the middle of the acquisition. The black arrows correspond to NaClO₄, NaI, or NaCl injections. Each value was calculated from three independent experiments.

Our data demonstrate that the kinetics of ^{99m}Tc pertechnetate uptake into the salivary glands and the stomach are slower than those of uptake into the thyroid. This difference could result from a higher transport activity of the thyroid compared with these two other tissues. In addition, the ratio between the number of NIS-expressing cells and the volume of the apical compartment differs between these organs. The fundamental functioning unit of the thyroid is the colloid-containing follicle. Colloid volume is much smaller than the gastric lumen and, therefore, should be more rapidly filled with isotope, although the bordering

epithelial cells may show a similar transport activity. As mentioned earlier, ^{99m}Tc pertechnetate uptake into the salivary glands is also relatively slower. In this tissue, only duct cells express NIS, and after uptake, the isotope then spreads first into the ducts and finally into the acini and the tubule system before the maximal, steady-state level of organ uptake is reached.

We also observed that the decrease in ^{99m}Tc pertechnetate uptake is faster in the thyroid than in the salivary glands or the stomach after injection of an excess of iodide or perchlorate. Both anions are competitive inhibitors of NIS and will block the active, NIS-mediated isotope accumulation. Differences in the kinetics of the decrease of the ^{99m}Tc pertechnetate uptake of these organs should result from differences in the isotope efflux rates, and again, the basic structure of each organ may play an important role. As expected, the passive efflux of ^{99m}Tc pertechnetate from the large gastric lumen is much slower than that from the thyroid's small follicles.

To compare this work with other *in vivo* imaging studies using radioactive iodide, it is important to take into account that radioactive iodide, in contrast with other NIS substrates, can be oxidized and bound to proteins and lipids. This incorporation of iodide into organic molecules is especially active in the thyroid, where it is a key process in hormone production. During this process, which takes place in the colloid, iodide is rapidly bound to the hormone precursor, thyroglobulin. Consequently, the quantity of accumulated iodide is not only correlated to its uptake equilibrium but rapidly corresponds to the amount of iodide that has been bound to thyroglobulin. Thus, in the thyroid, the kinetics of accumulated radioactivity will be different for ^{99m}Tc pertechnetate and ¹²³I iodine. Although organification of iodine has been described for the salivary glands, the process is not very efficient, and it can be ignored in comparison with the efficient organification in the thyroid. The effect of iodine organification has been illustrated by Zuckier *et al.* (16). These authors found that uptake kinetics in the salivary glands were similar for ¹²³I iodine, ^{99m}Tc pertechnetate, and ¹⁸⁸Re perrhenate. In the thyroid, however, the accumulation of ¹²³I iodine increased continuously, and 19 hours after injection, nearly the entire injected dose was found in this organ. The authors also confirmed this result by *in vivo* imaging.

Rocchi *et al.* attributed the radioactive iodide accumulation found in the neck region of mice to the unique uptake activity of the thyroid (25). Their approach may undoubtedly have no major consequences on the given results. As discussed earlier, several hours after injection of the radiotracer the portion of the radioactivity detected in the neck region, which is due to the uptake activity of the salivary glands, can be disregarded (20,26).

The mouse thyroid was distinguished from the salivary glands with a newly developed, small-animal-dedicated SPECT camera (27). However, as reported in this work, geometric calibration of a clinically dedicated camera with a pinhole collimator also allows the acquisition of SPECT images with the high resolution required for mouse imaging. We have shown that such high resolution is an important issue, not only for research on the thyroid but also for all studies using a gamma emitter as a signal for *in vivo* imaging. The cloning of the NIS cDNA now allows the

targeting of NIS expression into any cell type using gene therapy. This enables the targeted cells to accumulate iodide (via NIS) and they may then selectively be destroyed using radioiodide therapy. In addition, NIS can be used as a reporter gene in scintigraphic imaging for preclinical experiments. The use of our geometric calibration system of SPECT imaging will allow a more detailed and precise analysis of the NIS-expressing cell distribution in preclinical trials.

Acknowledgments

The authors thank Dr. Sabine Lindenthal and Dr. Patrick Chang for critical reading of the manuscript. This work was supported by grants from Electricité de France and "Conseil Général 06."

Disclosure Statement

The authors have no conflict of interest.

References

- Dohan O, De La Vieja A, Paroder V, Riedel C, Artani M, Reed M, Ginter CS, Carrasco N 2003 The sodium/iodide symporter (NIS): characterization, regulation, and medical significance. *Endocr Rev* **24**:48–77.
- Vayre L, Sabourin JC, Caillou B, Ducreux M, Schlumberger M, Bidart JM 1999 Immunohistochemical analysis of Na⁺/I-symporter distribution in human extra-thyroidal tissues. *Eur J Endocrinol* **141**:382–386.
- Weber DA, Ivanovic M, Franceschi D, Strand SE, Erlandsson K, Franceschi M, Atkins HL, Coderre JA, Susskind H, Button T, Ljunggren K 1994 Pinhole SPECT: an approach to *in vivo* high resolution SPECT imaging in small laboratory animals. *J Nucl Med* **35**:342–348.
- Beekman FJ, van der Have F, Vastenhouw B, van der Linden AJ, van Rijk PP, Burbach JP, Smidt MP 2005 U-SPECT-I: a novel system for submillimeter-resolution tomography with radiolabeled molecules in mice. *J Nucl Med* **46**:1194–1200.
- Funk T, Despres P, Barber WC, Shah KS, Hasegawa BH 2006 A multipinhole small animal SPECT system with submillimeter spatial resolution. *Med Phys* **33**:1259–1268.
- Walrand S, Jamar F, de Jong M, Pauwels S 2005 Evaluation of novel whole-body high-resolution rodent SPECT (Linoview) based on direct acquisition of linogram projections. *J Nucl Med* **46**:1872–1880.
- Defrise M, Vanhove C, Nuyts J 2008 Perturbative refinement of the geometric calibration in pinhole SPECT. *IEEE Trans Med Imaging* **27**:204–214.
- Beque D, Nuyts J, Bormans G, Suetens P, Dupont P 2003 Characterization of pinhole SPECT acquisition geometry. *IEEE Trans Med Imaging* **22**:599–612.
- Beque D, Nuyts J, Suetens P, Bormans G 2005 Optimization of geometrical calibration in pinhole SPECT. *IEEE Trans Med Imaging* **24**:180–190.
- Vanhove C, Defrise M, Franken PR, Everaert H, Deconinck F, Bossuyt A 2000 Interest of the ordered subsets expectation maximization (OS-EM) algorithm in pinhole single-photon emission tomography reconstruction: a phantom study. *Eur J Nucl Med* **27**:140–146.
- Vanhove C, Andreyev A, Defrise M, Nuyts J, Bossuyt A 2007 Resolution recovery in pinhole SPECT based on multi-ray projections: a phantom study. *Eur J Nucl Med Mol Imaging* **34**:170–180.
- Loening AM, Gambhir SS 2003 AMIDE: a free software tool for multimodality medical image analysis. *Mol Imaging* **2**:131–137.
- Perron B, Rodriguez AM, Leblanc G, Pourcher T 2001 Cloning of the mouse sodium iodide symporter (mNIS) and its expression in the mammary gland and other tissues. *J Endocrinol* **170**:185–196.
- Spitzweg C, Joba W, Eisenmenger W, Heufelder AE 1998 Analysis of human sodium iodide symporter gene expression in extrathyroidal tissues and cloning of its complementary deoxyribonucleic acids from salivary gland, mammary gland, and gastric mucosa. *J Clin Endocrinol Metab* **83**:1746–1751.
- Caillou B, Troalen F, Baudin E, Talbot M, Filetti S, Schlumberger M, Bidart JM 1998 Na⁺/I- symporter distribution in human thyroid tissues: an immunohistochemical study. *J Clin Endocrinol Metab* **83**:4102–4106.
- Zuckier LS, Dohan O, Li Y, Chang CJ, Carrasco N, Dadachova E 2004 Kinetics of perrhenate uptake and comparative biodistribution of perrhenate, pertechnetate, and iodide by NaI symporter-expressing tissues *in vivo*. *J Nucl Med* **45**:500–507.
- Barton KN, Tyson D, Stricker H, Lew YS, Heisey G, Koul S, de la Zerda A, Yin FF, Yan H, Nagaraja TN, Randall KA, Jin GK, Fenstermacher JD, Jhiang S, Ho Kim J, Freytag SO, Brown SL 2003 GENIS: gene expression of sodium iodide symporter for noninvasive imaging of gene therapy vectors and quantification of gene expression *in vivo*. *Mol Ther* **8**:508–518.
- Petrich T, Quintanilla-Martinez L, Korkmaz Z, Samson E, Helmeke HJ, Meyer GJ, Knapp WH, Potter E 2006 Effective cancer therapy with the alpha-particle emitter [211At]astatine in a mouse model of genetically modified sodium/iodide symporter-expressing tumors. *Clin Cancer Res* **12**:1342–1348.
- Dingli D, Peng KW, Harvey ME, Greipp PR, O'Connor MK, Cattaneo R, Morris JC, Russell SJ 2004 Image-guided radiotherapy for multiple myeloma using a recombinant measles virus expressing the thyroidal sodium iodide symporter. *Blood* **103**:1641–1646.
- Mandell RB, Mandell LZ, Link CJ Jr. 1999 Radioisotope concentrator gene therapy using the sodium/iodide symporter gene. *Cancer Res* **59**:661–668.
- Cho JY, Shen DH, Yang W, Williams B, Buckwalter TL, La Perle KM, Hinkle G, Pozderac R, Kloos R, Nagaraja HN, Barth RF, Jhiang SM 2002 *In vivo* imaging and radioiodine therapy following sodium iodide symporter gene transfer in animal model of intracerebral gliomas. *Gene Ther* **9**:1139–1145.
- Brown-Grant K 1963 Failure to demonstrate a concentration of iodide by the submandibular gland of the rat. *J Physiol* **165**:519–527.
- Cho JY, Leveille R, Kao R, Rousset B, Parlow AF, Burak WE Jr., Mazzaferri EL, Jhiang SM 2000 Hormonal regulation of radioiodide uptake activity and Na⁺/I- symporter expression in mammary glands. *J Clin Endocrinol Metab* **85**:2936–2943.
- Yang HS, Lee H, Kim SJ, Lee WW, Yang YJ, Moon DH, Park SW 2004 Imaging of human sodium-iodide symporter gene expression mediated by recombinant adenovirus in skeletal muscle of living rats. *Eur J Nucl Med Mol Imaging* **31**:1304–1311.
- Rocchi R, Kunavisarut T, Ladenson P, Caturegli P 2006 Thyroid uptake of radioactive iodine and scintigraphy in mice. *Thyroid* **16**:705–706.

26. Goel A, Carlson SK, Classic KL, Greiner S, Power AT, Bell JC, Russell SJ 2007 Radioiodide imaging and radiovirotherapy of multiple myeloma using VSV(Delta51)-NIS, an attenuated vesicular stomatitis virus encoding the sodium iodide symporter gene. *Blood* **110**:2342–2350.
27. Marsee DK, Shen DH, MacDonald LR, Vadysirisack DD, Lin X, Hinkle G, Kloos RT, Jhiang SM 2004 Imaging of metastatic pulmonary tumors following NIS gene transfer using single photon emission computed tomography. *Cancer Gene Ther* **11**:121–127.

Address correspondence to:
Thierry Pourcher, Ph.D.
TIRO
Faculté de Médecine
28 Ave. de Valombrose
06107 Nice
France

E-mail: pourcher@unice.fr